BMC Genomics

RESEARCH Open Access

A combined analysis of bulk RNA-seq and scRNA-seq was performed to investigate the molecular mechanisms associated with the occurrence of myocardial infarction

Zheng Xie[1], Huicong Xie[1], Chen Xie[1], Saichao Yang[1], Yun Feng[1], Zhaohai Su[2], Tao Tang[2], Bilong Zhang[2], Jiangyong Yang[2], Yueting Wang[2], Ling Huang[2], Hengqing Zhu[2], Jun Cao[2], Rengui Jiang[2], Tian Li[3] and Weiling Lu[2*]

Abstract

Background Myocardial infarction (MI) induces complex transcriptional changes across diverse cardiac cell types. Single-cell RNA sequencing (scRNA-seq) provides an unparalleled ability to discern cellular diversity during infarction, yet the veracity of these discoveries necessitates confirmation. This investigation sought to elucidate MI mechanisms by integrating scRNA-seq and bulk RNA-seq data.

Methods Publicly available scRNA-seq (GSE136088) and bulk RNA-seq (GSE153485) data from mice MI models were analyzed. Cell types were annotated, and differential expression analysis conducted. Bulk RNA-seq underwent quality control, principal component analysis, and differential expression analysis.

Results In scRNA-seq data, the comparison between MI and sham groups unveiled a reduction in endothelial cell populations, but macrophages and monocytes increased. Within fibroblast subgroups, three distinct categories were discerned, with two exhibiting upregulation in MI. Notably, endothelial cells exhibited an elevated expression of genes associated with apoptosis and ferroptosis. In bulk RNA-seq analysis, distinct patterns emerged when comparing MI and sham groups. Specifically, six genes linked to endothelial ferroptosis exhibited heightened expression in MI group, thereby corroborating the scRNA-seq findings. Moreover, the examination of isolated cardiac macrophages from mice MI model revealed increased expression of Spp1, Col1a2, Col3a1, Ctsd, and Lgals3 compared to sham group, thus substantiating the dysregulation of macrophage apoptosis-related proteins following MI.

Conclusion MI altered the transcriptomic landscapes of cardiac cells with increased expression of apoptotic genes. Moreover, the upregulation of macrophage apoptosis marker was confirmed within MI models. The presence of endothelial cell depletion and ferroptosis in MI has been demonstrated.

Keywords Myocardial infarction, scRNA-seq, Fibroblast, Macrophage, Ferroptosis

*Correspondence:
Weiling Lu
onlybei11@163.com
[1]Department of General Practice, Ganzhou Hospital of Guangdong Provincial People's Hospital, Ganzhou Municipal Hospital (Gannan Medical University Affiliated Municipal Hospital), 49 Dagong Road, Ganzhou 341000, China
[2]Department of Cardiology, Ganzhou Hospital of Guangdong Provincial People's Hospital, Ganzhou Municipal Hospital (Gannan Medical University Affiliated Municipal Hospital), 49 Dagong Road, Ganzhou 341000, China
[3]School of Basic Medicine, Fourth Military Medical University, Xi'an 710032, China

Background

Cardiovascular diseases remain the main killer worldwide [1–5]. Myocardial infarction (MI), colloquially referred to as a heart attack, remains a significant global public health challenge and a primary cause of mortality [6–9]. Recent studies estimate the annual incidence of MI to be 650,000 cases in the United States and over 7 million cases worldwide [10, 11]. Epidemiological data indicate the incidence has declined in high-income countries over the past two decades, largely attributed to improvements in preventive care, though MI still causes approximately 1 in every 16 deaths in the U.S [12]. The prevalence of MI among adults hovers approximately 3%, with a higher incidence among men compared to women across most age brackets. Nevertheless, research indicates that women tend to experience their first MI at an older age and face a higher associated mortality rate than men [13].

Well-established risk factors such as smoking, hypertension, diabetes, and hyperlipidemia are responsible for the majority of MI, yet a significant portion, ranging from 25 to 30% of cases remain inexplicable [14]. Although there have been remarkable advancements in medical and interventional therapies, leading to substantial improvements in the short-term prognosis, it is disconcerting that nearly 20% of MI patients still succumb within a year, while recurrence affects around 5–20% within 12 months [15]. Ongoing research endeavors are diligently striving to achieve several critical objectives: to enhance our understanding of populations at risk, elucidate novel mechanisms and risk factors, optimize management strategies, and ultimately reduce the substantial morbidity and mortality that continue to result from MI.

Single-cell RNA sequencing has emerged as a transformative technological paradigm in the domain of cardiovascular research, providing unprecedented resolution of cellular heterogeneity and dynamic transcriptional processes in models of MI [16–19]. The application of single-cell sequencing to comprehensively profile diverse cardiac cell populations during infarction and subsequent remodeling has nominated regulatory pathways, intricate intercellular crosstalk mechanisms, and novel therapeutic targets that underpin the progression of this disease [20, 21]. Macrophage is a type of white blood cell located within tissues [22–25]. For instance, analyses have revealed MI-induced shifts in macrophages toward pro-inflammatory, profibrotic states, while also implicating specific endothelial, fibroblast, and cardiomyocyte subpopulations in maladaptive ventricular remodeling [26, 27]. However, it is imperative to acknowledge that the comprehensive exploration of these rich datasets necessitates further in-depth scrutiny through re-analysis. Initial investigations tend to concentrate solely on specific cell clusters and canonical markers during the preliminary data processing stages. Therefore, additional single-cell profiling of understudied cell types across more timepoints post-MI would provide a more complete picture. Critically, findings from bioinformatic analyses require validation by orthogonal methods such as bulk RNA sequencing, qRT-PCR, and western blotting in relevant animal models before conclusions can be drawn. It is through the synthesis of scRNA-seq with complementary approaches encompassing transcriptional, proteomic, and functional dimensions that the emerging regulatory mechanisms underlying MI can be robustly authenticated, thus paving the way for the translation of these insights into novel therapeutic strategies for the benefit of patients.

Methods

Data source

Reading keywords and abstracts, six datasets GSE136088, GSE153485, GSE60993, GSE61144, GSE186079 and GSE123342 were found in the public database GEO. GSE136088 utilized the Illumina HiSeq 2500 platform to perform DropSeq scRNA-seq analysis on 1 case of MI and 1 case of control group mouse heart samples. GSE153485, employing the Illumina NovaSeq 6000 platform, conducted bulk RNA-seq on 10 mouse heart samples. Out of these, 5 samples were from the MI group, while the remaining 5 were from the control group. GSE60993 utilized the Illumina HumanWG-6 v3.0 expression beadchip to perform transcriptome analysis on ST-elevation MI (STEMI) 7 samples, non-ST-elevation MI (NSTEMI) 10 samples and unstable angina (UA) 9 samples, and normal control 7 samples. GSE61144 utilized the Sentrix Human-6 v2 expression beadchip to perform transcriptome analysis on a set of blood samples of patients with STEMI 7 samples before and 7 days after the primary percutaneous coronary intervention 7 samples and normal control 10 samples. GSE186079 utilized the Illumina HiSeq 4000 platform to perform ATAC-seq amd RNA-seq. GSE123342 utilized the Affymetrix human transcriptome array 2.0 platform to perform peripheral blood RNA profiling in 192 samples, including acute MI 65 samples, 30 days post-MI 64 samples, 1 year post-MI 37 samples, patients with stable CAD 22 samples and technical replicates 4 samples.

Bulk RNA-seq data analysis

In bulk RNA-seq dataset, to synthesize cDNA, a high-capacity cDNA reverse transcription kit (#4368814, Applied Biosystems, USA) was utilized in conjunction with random primers. For the analysis of mRNA expression of genes of interest, TaqMan real-time PCR was performed on the ViiA 7 System (Applied Biosystems, USA). Poly-A selection was adopted in Illumina RNA-seq to prepare RNA sequencing libraries. Subsequently, these

libraries were sequenced on the NovaSeq6000 platform (NovaSeq Control Software 1.6.0/RNA v3.4.4). To filter protein-coding genes and transcripts, we performed mapping using localization files retrieved from the Ensembl BioMart website to assign transcripts to genes. Genes with average expression levels less than 1 transcripts per million (TPM) in all conditions were excluded from further analysis [28]. To analyze bulk RNA-seq data, quality control was firstly performed and then Principal Component Analysis (PCA) was applied utilizing R programming. Wilcoxon non-parametric test was employed to compare the significance of gene expression differences between the two groups.

scRNA-seq data analysis

We downloaded the single-cell transcriptome data GSE136088 from the GEO database, which included one MI mouse model and a control group. The heart tissues were collected at 14th day of post-Sham surgery or MI. The scRNA-seq data was analyzed using Seurat package. The scater method was employed to filter out outlier gene expressions values (MADs=3), excluding low-quality cells based on the following criteria: excluding low-quality cells based on the following criteria: (I) reads were filtered based on Phred quality scores, with reads discarded if the Phred score was <30; (II) cells with fewer than 5 detected genes or fewer than 200 total detected genes were excluded; (III) cells with a mitochondrial gene expression proportion of ≥20% were excluded [29]. The ScaleData function was used to normalise gene expression values according to sequencing library size, and the IntegrateData function was used to merge single-cell expression matrices from different samples. In addition, Scrublet was used to identify double dots by simulating and calculating the probability of double dots for each cell. Cells with a high probability of double parietal bodies were excluded from the dataset. To identify genes that were significantly differentially expressed in different cell populations, differential gene expression analysis was conducted on the scRNA-seq dataset using Seurat. To control the error rate, Bonferroni corrections for strict multiple testing were applied. To obtain meaningful cell clustering results, a resolution of 0.1 was chosen for t-SNE clustering analysis. The singleR package was utilized for single-cell annotation. Differential gene expression analysis was performed by comparing gene expression among different cell clusters (pct>0.2, min. cells=3, avg_log2FC>0.25 or < -0.25). Finally, K-means clustering was used to group cells based on marker genes and characterise each group. Similarly, the Clusterprofiler package was used for functional annotation of differential expression gene (DEGs).

Animals

Healthy male C57BL/6 mice, aged between 6 and 8 weeks, were chosen to establish a MI model. These mice were sourced from Guangdong Vital River Laboratory Animal Technology in Guangzhou and maintained at the Biomedical Animal Research Facility of Gannan Medical University, which meets SPF standards. Our team strictly adhered to established guidelines for the humane treatment and care of lab animals. All the procedures and housing conditions for the mice were in line with the standards set by Gannan Medical University. The study obtained the necessary clearance from the university's Institutional Ethics Committee, in compliance with the directives stipulated by the Ministry of Science and Technology emphasizing the humane handling of experimental animals. The ethical clearance for our research was secured from the Ethical Committee of Gannan Medical University, under the reference number: 2,023,555.

Establishment of MI model

C57BL/6 male mice aged 8 weeks were used to establish MI models; the weight of mice in constructing the MI model was 21–27 g. After 0.4 L/min of isoflurane gas anesthesia, the chest/armpit hair was removed. After anesthesia with 0.4 L/min of isoflurane gas, the chest was opened to expose the heart, and a small pericardial section below the left atrium was made to expose and ligate the left anterior descending coronary artery (LAD). Under a microscope, the LAD's course or location was identified. Using a 7−0 suture and needle holder, blood flow in the LAD was completely occluded approximately 2 mm below the left atrium. After ligation, the chest was sutured layer by layer and postoperative monitoring maintained for breathing abnormalities or condition changes.

Once conscious, mice were extubated and returned to normal housing. In the Sham group, the chest was opened, but no LAD blood flow blockage was performed. Hearts were collected at 14th day of post-Sham surgery or MI, Post-surgery, both MI and Sham group mice underwent electrocardiograms and cardiac ultrasounds to analyze left ventricular function. Opted the method of inducing euthanasia in mice by administering an overdose of inhaled isoflurane. The specific steps are the following: Prepare a closed container with a layer of absorbent, pour the isoflurane on the absorbent, and place the mice into the container. Cover the lid of the container to ensure that the container is well sealed and to prevent isoflurane leakage. Gradually increase the concentration of isoflurane and observe the behavioral and physiological responses of the mice to confirm their gradual loss of consciousness and eventually death. Then, the heartbeat and breath were checked for physical death confirmation. Finally, collect heart tissues of mice. The

heart tissues were collected at 14th day after sham surgery or MI for follow-up experiments, perfuse with ice-cold PBS to remove red blood cells followed by perfusion with 50 mM KCl to arrest the heart in diastole and then fixed for 4 h in freshly prepared 4% Paraformaldehyde (PFA) at 4 °C, rinsed with PBS and cryoprotected in 30% sucrose/PBS overnight before embedding in Optimal cutting temperature compound (OCT).

Isolation of macrophages

After collecting the heart tissue, we used scissors to cut the paper towel into small pieces of 2–4 mm, then we added tissue protease and incubated at 37 ℃ until dispersed. The digested tissue was filtered using a 70 μm-filter, and the filtered cell suspension was collected into a new centrifuge tube. Centrifuged at 300 g for 4–5 min at 4 ℃, discarded the supernatant, and resuspended cell pellet in PBS. This step should be repeated 3 times. The cardiomyocyte suspension was carefully spread on a Percoll gradient in a 50 mL centrifuge tube with 25% and 70% Percoll solutions and centrifuged at 800 g for 20 min. Macrophages were concentrated at the gradient interface, washed twice with cold PBS, centrifuged at 300 g for 5 min, and the supernatant was discarded. Incubated cells with PE-labeled anti-F4/80 (#565410, Becton-Dickinson, San Jose, CA) and FITC-labeled anti-CD11b antibody (#557396, Becton-Dickinson, San Jose, CA) dilutions at 4 ℃. After incubation, cells were used for flow cytometry and only double-positive cells were collected. The purified macrophages were cultured in a 37 ℃ incubator for subsequent experiments.

Echocardiography in mice

Echocardiographic examinations were performed using the VisualSonics VEVO 2100 system (VisualSonics Inc., Ontario, Canada). At 24 h post-MI, infarcted areas were calculated based on the wall motion scoring index (WMSI) using a 16-segment model across three short-axis images, where a score of 0 represents normal, 0.5 for reduced wall thickening and excursion within a segment, and 1 for no wall thickening and excursion within a segment. The WMSI was calculated as the sum of the scores divided by the total number of segments. Before imaging, depilatory gel was applied to the chest of the isoflurane-anesthetized (1.2%) mice to reduce resistance to ultrasonic beam transmission. Mice were anesthetized with isoflurane as described above. The mice were then placed on a heating pad and their limbs were connected to an electrocardiogram. Imaging was performed using a 55 MHz linear transducer (MS550D). The data was evaluated using the VevoStrain software system (Visualsonics Inc., Ontario, Canada).

Histological detection

Mice hearts were excised at 14th day after MI, fixed with paraformaldehyde, embedded in paraffin, and sliced into 5 μm sections. After removing the paraffin, the hearts were stained with Masson's solution, differentiated by 1% hydrochloric acid alcohol, and stained with Ponceau's acid magentafor 5–10 min, followed by a quick rinse with distilled water. After treatment with aqueous phosphomolybdic acid for 3–5 min, the sections were counterstained with aniline blue solution for 5 min. After treatment with 1% glacial acetic acid for 1 min, the sections were dehydrated, dried and sealed for light microscopic.

Western blot

Macrophages were lysed with a lysis buffer for protein extraction. Protein concentrations were determined using the BCA assay, and a loading buffer was added. After heating and cooling, a 10% separation gel and a 5% stacking gel were prepared. Equal protein samples were loaded into wells. Electrophoresis was performed at constant voltages: 80 V for 30 min and 120 V for 90 min. Post-electrophoresis, the gel was cut, and proteins were transferred to a PVDF membrane over 2 h at 250 mA. The PVDF membrane was blocked with a 5% skim milk solution at room temperature for 2 h with gentle shaking. It was then washed three times with 1× TBST. The membrane was then incubated with primary antibodies anti-Spp1 (#PA5-34579, Invitrogen, Waltham, Massachusetts, USA, 1:1000), anti-Col1a2 (#PA1-26204, Invitrogen, Waltham, Massachusetts, USA, 1:1000), anti-Col3a1 (#PA5-34787, Invitrogen, Waltham, Massachusetts, USA, 1:2000), anti-Lgals3 (#ab217572, Abcam, Cambridge, UK, 1:1000), anti-Ctsd (#ab75852, Abcam, Cambridge, UK; 1:2000), anti-Ctsl (#ab200738,Abcam, Cambridge, UK; 1:1000), anti-β-Actin (#66009-1-IG, Proteintech, 1:1000) at 4 ℃ with gentle shaking overnight. The membrane was washed with 1× TBST and then incubated with secondary antibodies (Jackson ImmunoResearch Laboratories, anti-rabbit [111-035-047], 1:5000, and anti-rat [112-035-003], 1:5000) at 4 ℃ with gentle shaking for 2 h. Post-incubation, the membrane was washed 3 times with 1× TBST (5 min each). Images were acquired using SuperSignal West Pico Plus Chemiluminescent Substrate (#34578, Thermo Fisher Scientific, USA) via a ChemiDoc MP system (Bio-Rad Laboratories, CA, USA).

Quantitative Real Time PCR (qRT-PCR)

RNeasy Mini Kit Reagent (#74104, Qiagen, Germany) was used to extract the total RNAs of collected macrophages. First-strand cDNA was reverse-transcribed by High-Capacity cDNA Reverse Transcription kit (#4368814, Thermo Fisher Scientific, Carlsbad, CA). qRT-PCR was performed using a iTaq™ Universal SYBR®

Green Supermix kit (#1725121, Bio-Rad Laboratories, CA, USA). The qRT-PCR conditions were as follows: 95 ℃ for 8 min, 40 cycles of 95 ℃ for 10 s, 58 ℃ for 30 s, and 72 ℃ for 36 s. As β-actin was used as an internal control, $2^{-\Delta\Delta Ct}$ method was used to calculate the relative expression level of target genes. Each gene was tested three times independently. The sequence-specific primers of Spp1, Col1a2, Col3a1, Ctsd, Ctsl and Lgals3 were synthesized and the specific sequence of primers were showed in Table S1.

Statistical analysis

Statistical analyses were executed using IBM SPSS Statistics software (Version 26.0; IBM Corp., Armonk, NY, USA) and GraphPad Prism software (Version 9.0; GraphPad Software, Inc., La Jolla, CA, USA). Data distributions were initially verified for normality utilizing the Shapiro-Wilk test. Subsequently, either the Student's t-test (for comparisons between two groups) or one-way ANOVA followed by post-hoc tests (for multiple group comparisons) was employed. Data are presented as mean±standard deviation (SD). The statistical significance level was predetermined at $p<0.05$. Correlation analyses were performed using Pearson's or Spearman's rank correlation, based on the data distribution.

Results

Main cell types in MI mice

GSE136088 included scRNA-seq data from 1 MI mouse and 1 control mouse. After cell quality control, the MI group had 16,348 cells and 8,152 genes, and the sham group had 15,131 cells and 6,162 genes. Cells in both groups were annotated into 5 cell types: endothelial cells, fibroblasts, macrophages, monocytes, and stromal cells (Fig. 1). Furthermore, the set of cardiomyocyte-specific marker genes used during cell type annotation showed low expression levels in the sequencing data, leading to the exclusion of isolated cardiomyocytes from

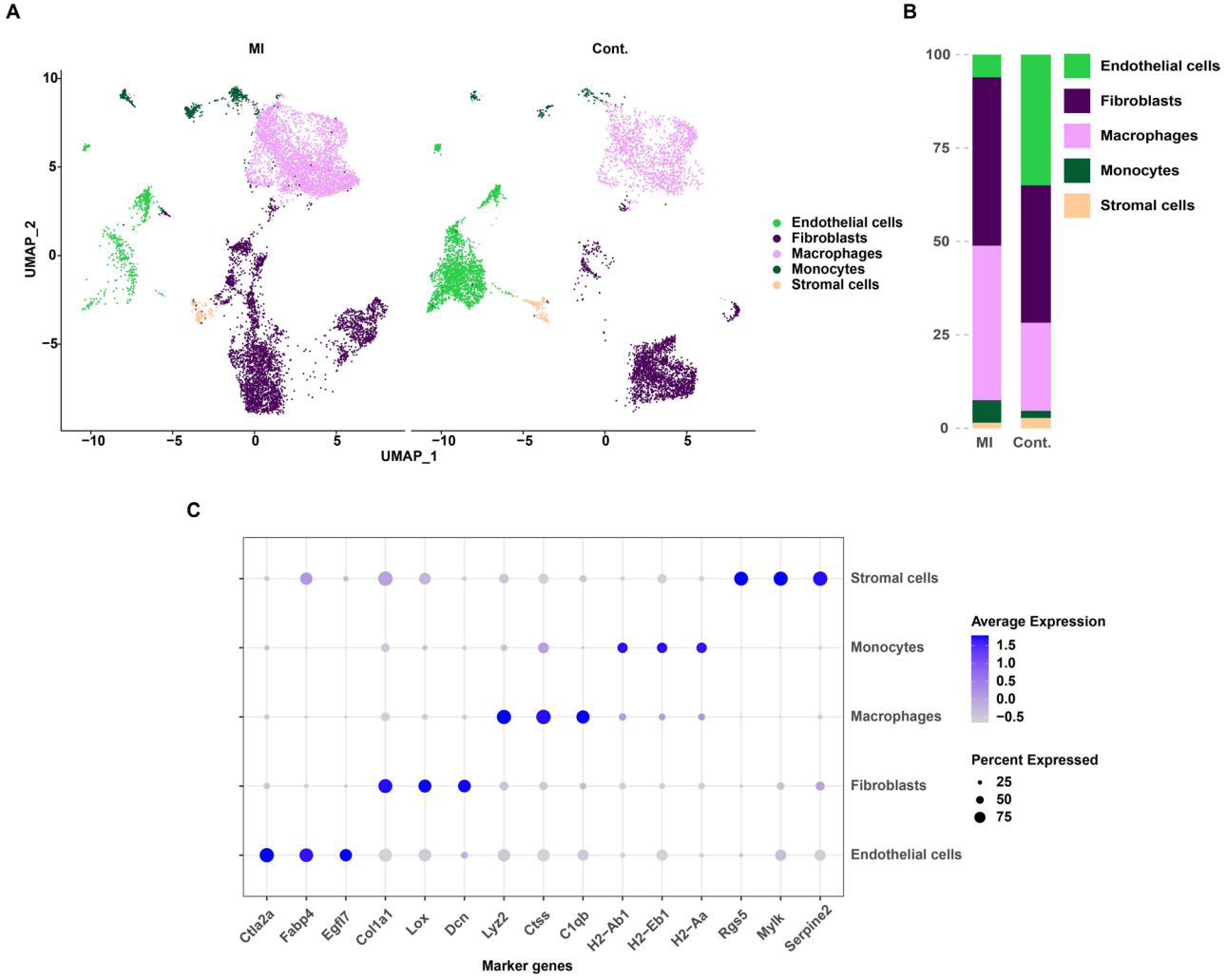

Fig. 1 Main cell types in GSE136088 datase. (**A**) Single-cell annotation results of two groups; (**B**) Proportions of different cell types in the two groups; (**C**) Expression of marker genes in various cell types

further analyses. In MI group, the major cell types were fibroblasts and macrophages, accounting for 45.08% and 41.36% respectively. In the control group, the predominant cell types were endothelial cells, fibroblasts, and macrophages, representing proportions of 34.96%, 36.81%, and 23.56% respectively (Table 1). The proportion of endothelial cells was significantly lower in MI group compared with control group, potentially related to apoptosis of endothelial cells following MI. On the other hand, the proportions of macrophages and monocytes were notably higher in MI group, possibly associated with post-infarction inflammatory responses. As the predominant cell type, fibroblasts showed no significant differences in composition between the two groups.

Three subgroups were identified within the fibroblast

To explore the role of fibroblasts in MI, we further analyzed of scRNA-seq data (GSE136088) revealed that myocardial fibroblasts secreted a large number of cytokines, chemokines, and growth factors to participate in the tissue repair process after MI. According to GSE136088 dataset, by analyzing the levels of Col1a1 and Col3a1, we observed an increase in the expression of collagen type I and III proteins (Fig. 2A) in the MI groups. Fibroblasts likely participated in cardiac repair after MI by enhancing the synthesis of collagen types I and III. According to the UMAP clustering analysis results (Fig. 2B-C; Table 2), three subgroups were identified within the fibroblast population. Two subgroups (S2, S3) showed significant increases in MI group, potentially related to post-MI cardiac repair. Functional annotation of the three fibroblast subgroups revealed that subgroups S1 and S2 might be associated with post-MI inflammatory responses and injury repair processes, including cell chemotaxis, wound healing, and leukocyte migration/ chemotaxis. On the other hand, subgroup S3 could be linked to post-MI fibroblast proliferation, involving processes such as nuclear division and chromosome segregation. Additionally, subgroups S1 and S2 were involved in the secretion of extracellular matrix proteins and the composition of the matrix, as indicated by extracellular matrix organization (Fig. 2D and E).

Table 1 In both MI and control group, the proportions of various types

	MI	Sham
Endothelial cells	511 (6.06%)	2180 (34.96%)
Fibroblasts	3803 (45.08%)	2295 (36.81%)
Macrophages	3489 (41.36%)	1469 (23.56%)
Monocytes	508 (6.02%)	120 (1.92%)
Stromal cells	125 (1.48%)	171 (2.74%)

MI occurrence involved multiple biological functions of endothelial cells

Endothelial cells regulated vascular dilation and tension by secreting vasoactive compounds and growth factors. Dysfunction of endothelial cells could be observed in atherosclerotic plaques, congestive heart failure (HF), and atrial fibrillation within the heart. In MI mice, a significant reduction in the proportion of endothelial cells was also observed in scRNA-seq data (GSE136088) (Fig. 1B). With p value <0.05, avg log2FC >0.25 or < -0.25, most genes expressed by endothelial cells were upregulated, which were also associated with cellular apoptosis and ferroptosis (Fig. 3A and B). Functional analysis (Fig. 3C and D) of these DEGs showed that, at the biological process level, these genes were predominantly enriched in pathways related to vascular development, such as regulation of vasculature development and regulation of angiogenesis, indicating the potential involvement of endothelial cells in the development of MI through the regulation of blood vessel formation. Furthermore, these DEGs were also related to epithelial cell migration and epithelium migration. This may be linked to the transient mesenchymal activation observed in endothelial cells after the occurrence of MI, as suggested by Tombor et al. Regarding KEGG analysis, it was found that the DEGs within endothelial cells were significantly enriched in pathways associated with heart-related diseases or functions, including diabetic cardiomyopathy and cardiac muscle contraction. This suggested that endothelial cells might play a role in the occurrence of MI from multiple levels.

Combined analyses of bulk RNA-seq and scRNA-seq data

Based on the analysis of scRNA-seq data, we further integrated bulk RNA-seq data to investigate the mechanisms associated with the occurrence and development of MI. According to GSE153485 dataset, PCA analysis of bulk RNA-seq data revealed there were no outlier (Fig. 4A). MI and the control group formed distinct clusters, indicating that the hearts of MI mice exhibited unique characteristics. Though scRNA-seq data analysis, we identified six genes that could potentially be involved in ferroptosis within endothelial cells. These genes were Fth1, Prnp, Vdac2, Sat1, Cp, and Gclm (Fig. 3C). We found that, except for Cp, all of these genes exhibited significantly higher expression in MI group of bulk RNA-seq data (Fig. 4B). Moreover, the analysis of scRNA-seq data also indicated significantly elevated expression of ferroptosis-associated genes in both endothelial cells and stromal cells (Fig. 4C), consistent with the findings from the bulk RNA-seq analysis. This collective evidence strongly suggested a potential correlation between the occurrence of MI and ferroptosis within endothelial cells.

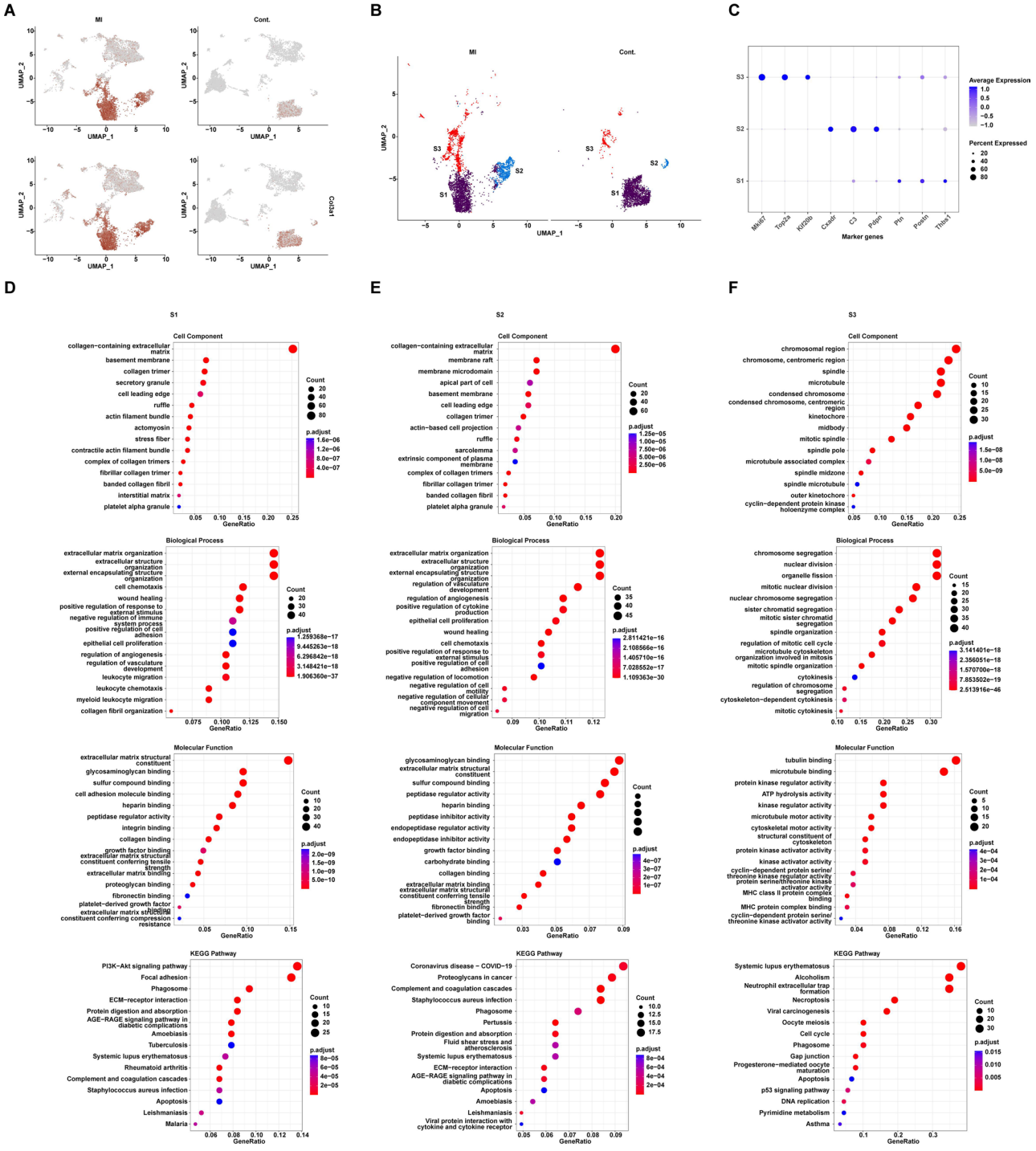

Fig. 2 Three subgroups were identified within the fibroblast. (**A**) The expression of type I and type III collagen proteins increased in fibroblasts in the MI group. (**B**) Different subtypes of fibroblasts. (**C**) Expression levels of marker genes in SI, S2, and S3 subtype. GO and KEGG analysis of (**D**) S1, (**E**) S2 and (**F**) S3

Table 2 In MI and control groups, the proportions of S1, S2 and S3

	MI	Sham
S1	2246 (59.06%)	2024 (88.19%)
S2	624 (16.41%)	96 (4.18%)
S3	933 (24.53%)	175 (7.63%)

Apoptotic changes in macrophages in MI

Macrophages are able to non-specifically recognize pathogens or cellular debris and activate lymphocytes or other immune cells to initiate an immune response. Following the occurrence of MI, there was a significant increase in the proportion of macrophages. This increase

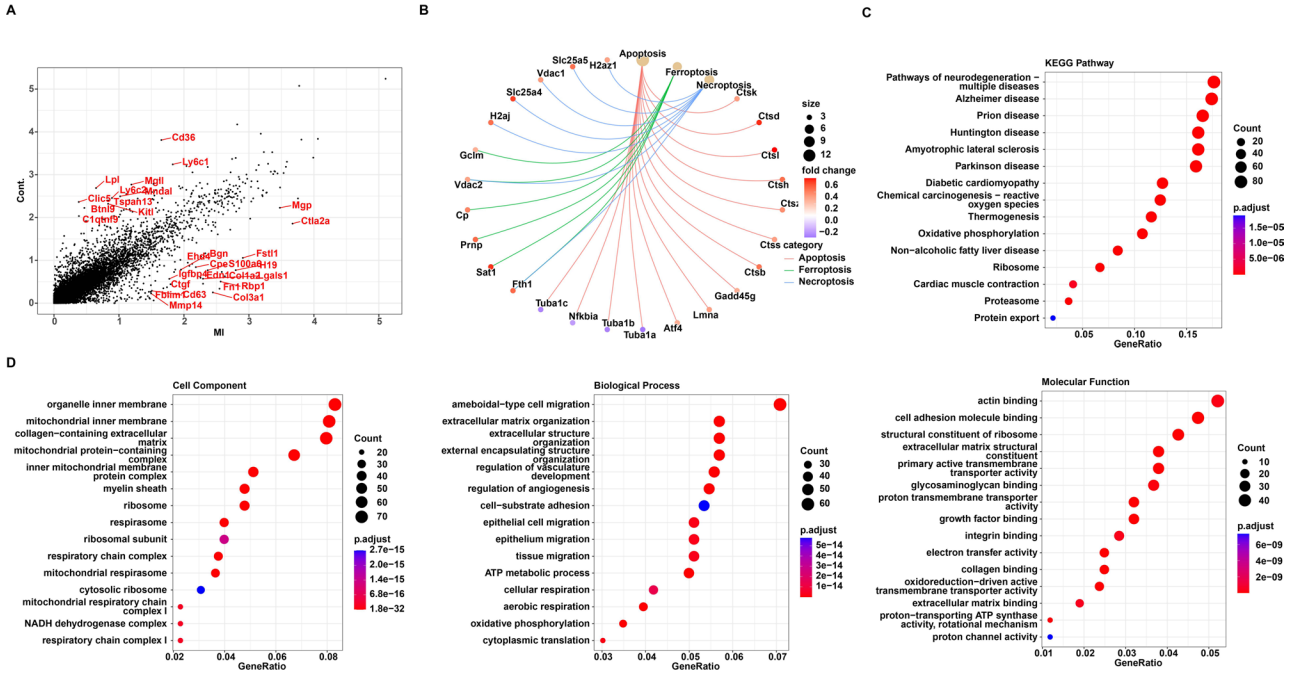

Fig. 3 MI occurrence involved multiple biological functions of endothelial cells. (**A**) DEGs in endothelial cells of MI group; (**B**) Apoptosis/ferroptosis-related network in endothelial cells; (**C**) KEGG and (**D**) GO enrichment analysis of DEGs in endothelial cells

might have been associated with the clearance of damaged cells and cellular debris.

We identified DEGs in Macrophages (p.value < 0.05, avg_log2FC > 0.25 or < -0.25). Genes such as Spp1, Col1a2, Col3a1, Ctsd, Ctsl, and Lgals3 were found to be highly expressed in MI group within Macrophages (Fig. 5A). Functional analysis of the DEGs revealed a close association between Ctsd, Ctsl, and apoptosis (Figure S1). According to the results of GO and KEGG enrichment analyses, at the cell component level, the DEGs were primarily concentrated in organelles related to cellular engulfment and degradation, such as endosomes and lysosomes. At the biological process level, these genes were involved in physiological functions such as leukocyte migration, cell chemotaxis, and leukocyte chemotaxis, contributing to immune recognition and clearance by macrophages. Similarly, in terms of molecular function, the DEGs were enriched in molecular functions like cytokine receptor binding and sulfur compound binding. In KEGG pathways, the DEGs in macrophages were significantly enriched in pathways related to immune responses, such as antigen processing and presentation, and lysosome (Figure S2). Following MI, macrophages were recruited to the site of heart tissue injury and further activated to play a role in tissue damage clearance and immune response.

To further investigate the relationship between DEGs and apoptosis in macrophages following MI, we established MI mice model to validate the sequencing results. We collected samples and performed echocardiography at 14th day after MI. As shown in Fig. 5B, our experiments indicated that mice in the MI group exhibited significant ST-segment elevation and altered T waves in their electrocardiograms, while no evident abnormalities were observed in the Sham group. Additionally, the cardiac ultrasound results showed a significant decrease in left ventricular ejection fraction (LVEF) and left ventricular shortening fraction (LVSF) in the MI group compared to the Sham group (Fig. 5C and D). Moreover, masson staining showed that collagen deposition and the expansion of myocardial fibrosis area, indicating that myocardial necrosis was confirmed in MI group compared with control (Fig. 5E). Taken together, we successfully established MI model. We next isolated cardiac macrophages from both groups of mice (Figure S3) and found that in the MI group, the expression levels of Spp1, Col1a2, Col3a1, Ctsd, and Lgals3 were upregulated, while the expression of Ctsl showed no significant change (Fig. 5F-H).

We showed the expression trends of Spp1, Col1a2, Col3a1, Ctsd, and Lgals3 at early and late time points after MI by analyzing GSE186079 and GSE123342 datasets. As shown in Figure S4A, the expression of Spp1 showed significantly higher expression levels compared to other groups, with the highest expression on the 7th day. The expression of Lgals3 was elevated on both day 3 and day 7 after MI. In the GSE123342 dataset, the expression of Spp1 and Ctsd decreased in Figure S4B, and the expression of Col1a2 and Col3a1 increased on the 30th day and decreased one year later. The expression of

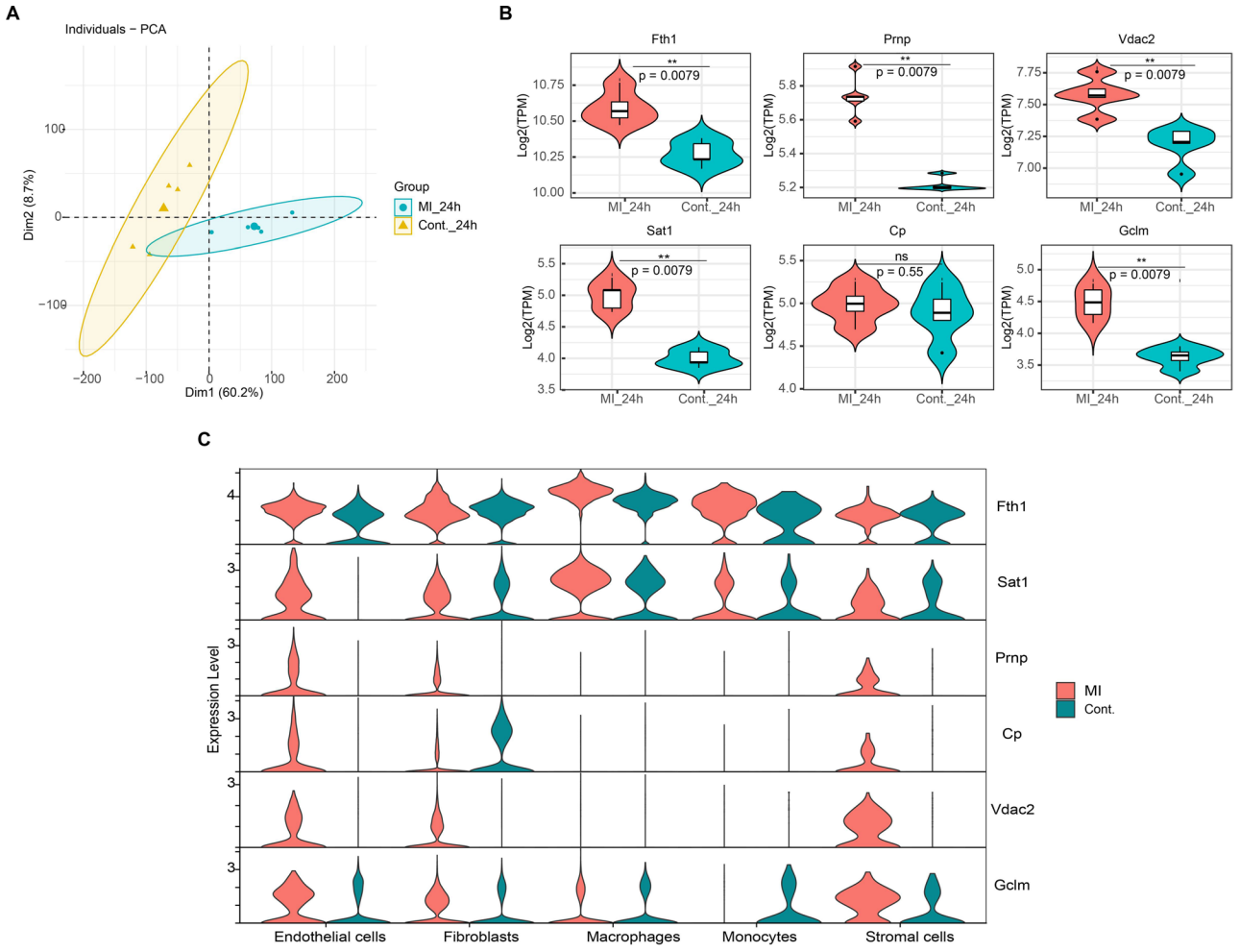

Fig. 4 Combined analyses of bulk RNA-seq and scRNA-seq data. (**A**) PCA analysis of bulk RNA-seq data; (**B**) Elevated expression of ferroptosis-related genes in bulk RNA-seq; (**C**) Elevated expression of ferroptosis-related genes in scRNA-seq data

Lgals3 gradually increased and leveled off in the first year. Additionally, we identified the above DEGs in human datasets GSE60993 and GSE61144. As shown in Figure S5, compared to sham group, the expression levels of Spp1 and Ctsd were significantly up-regulated after MI, while the differences of Col1a2, Col3a1 and Lgals3 were not significant.

In addition, to elucidate the molecular mechanism of the interaction between these genes, and the mechanism by which macrophages may regulate autophagy of cardiomyocytes through the secretion of Ctsd, we analyzed the human dataset GSE60993. Down-regulated top20 genes on DEGs were selected for protein-protein interaction (PPI) network analysis at https://cn.string-db.org/, The PPI network analysis revealed that the key molecules of interest in macrophages were Spp1, Col1a2, Col3a1, Ctsd and Lgals3 (Figure S6A). Moreover, gene set enrichment analysis (GSEA) was performed using GSEA v4.3.3, based on KEGG and GO databases, with gene expression levels in high and low Ctsd expression groups (median) in the GSE60993 dataset. The results showed that Ctsd was significantly enriched in the autophagy pathway (Figure S6B). Thus, the results of our analysis were consistent with previous studies indicating that Ctsd plays a role in autophagy related mechanisms.

This was consistent with the above-mentioned bioinformation analysis results, further confirming the abnormal levels of apoptosis-related proteins in murine macrophages during MI. Moreover, Spp1 and Ctsd were more significant in clinical relevance.

Discussion

Main interpretation

In this study, we performed an integrated analysis of bulk RNA-seq and scRNA-seq data to investigate the transcriptional mechanisms associated with MI pathogenesis. Our results demonstrated that MI induced substantial influences on both the composition and transcriptomic profiles of diverse cardiac cell populations, encompassing endothelial cells, fibroblasts, and macrophages.

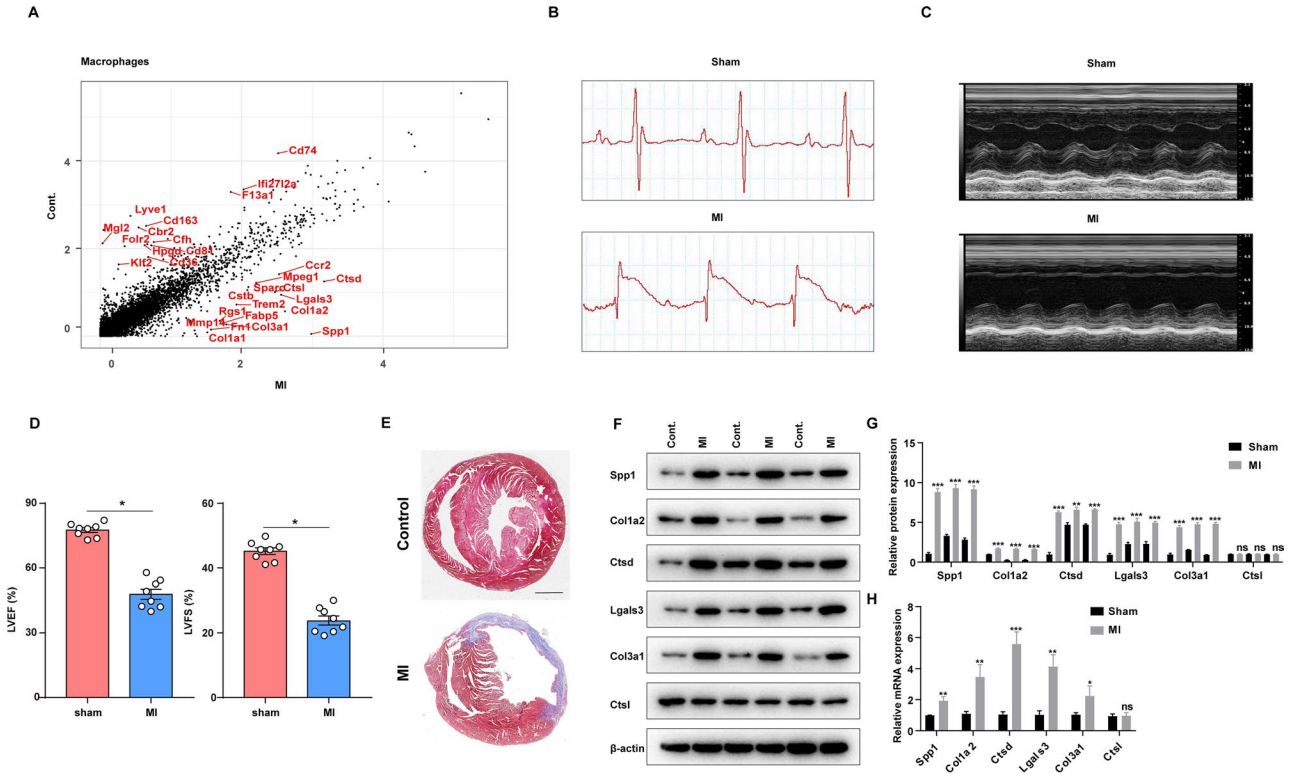

Fig. 5 Apoptotic changes in macrophages in MI. (**A**) DEGs in macrophages; (**B**) Representative electrocardiograms of mice in the Sham and MI group after modeling completion; (**C**) Representative cardiac ultrasound images of mice in the Sham and MI group on the first day after modeling; (**D**) LVEF and LVSF of mice in the Sham and MI group; ($n=8$ per group); (**E**) Representative masson staining diagrams in the control and MI group; scale bar = 1.5 mm; ($n=1$ per group); (**F**) Protein levels of Spp1, Col1a2, Ctsd, Lgals3, Col3a1, and Ctsl in MI mice heart macrophages; ($n=3$ per group); (**G**) Statistical analyses of (**E**); ($n=3$ per group); (**H**) The mRNA levels of Spp1, Col1a2, Ctsd, Lgals3, Col3a1, and Ctsl in MI mice heart macrophages; ($n=6$ per group); $^{*}p \le 0.05$; $^{**}p \le 0.01$; $^{***}p \le 0.001$

Consistent with previous studies [16, 17], we identified elevated expression of profibrotic genes such as Col1a1/Col3a1 accompanied by discernible shifts in the proportions of fibroblast subclusters involved in extracellular matrix deposition and the wound healing response following MI. Additionally, our observations indicated a decline in the number of endothelial cells, concomitant with heightened expression of genes implicated in apoptosis and ferroptosis, thus intimating the potential involvement of endothelial cell death contributes to infarction. Significantly, our integrated analysis, which merged scRNA-seq and bulk RNA-seq data, furnished compelling cumulative evidence substantiating the role of ferroptosis in the etiology of MI.

In macrophage populations, we found that MI induced an increase in the proportion of tissue damage-clearing and immune-responsive subpopulations, as well as an increase expression levels of specific genes, particularly Spp1, Col1a2, Col3a1, Ctsd, and Lgals3. We confirmed apoptosis-related Ctsd was upregulated in isolated cardiac macrophages from our MI mouse model. Overall, our comprehensive multi-omics approach elucidated MI-associated gene expression changes in diverse cardiac cell types. However, it is crucial to emphasize the imperative need for further validation to substantiate these findings rigorously.

Spp1, encodes osteopontin (OPN), played a pivotal role in tissue repair and fibrosis processes following MI. Notably, OPN is primarily expressed by macrophages characterized by the presence of Lgals3 and CD206 markers. Furthermore, it has been elucidated that interleukin-10 (IL-10) can promote the differentiation of cardiac macrophages into Spp1-expressing reparative cells, and MerTK expression is also associated with Spp1 transcriptional activation [30, 31]. Our research has drawn the same result that the expression level of Spp1 in isolated macrophages increased, suggesting that Spp1 plays a key role in tissue repair after MI.

Col1a2, encoding the α2 chain of type I collagen, assumed a critical role in the context of cardiac health. Notably, mutations in Col1a2 have been linked to conditions such as aortic dissection and coronary artery dissection. Increased expression of Col1a2 is also associated with myocardial fibrosis after MI [32–34]. Given the elevated expression of Col1a2 in isolated macrophages

post-MI, we inferred that Col1a2 plays a role in cardiac health after MI.

Ctsd, an essential lysosomal protease, played a pivotal role in maintaining intracellular environmental homeostasis. A growing number of studies have revealed the significance of Ctsd in MI, HF, and cardiac function. After MI, autophagy of cardiomyocytes is activated in response to ischemic injury, and Ctsd exerted a protective role in myocardial remodeling post-injury. This increased expression of cathepsin D serves to promotes autophagic flux, thereby playing a protective role in safeguarding cardiomyocytes [35]. The absence of Ctsd exacerbates cardiac remodeling subsequent to MI [36, 37]. In HF, significant alterations in the expression and activity of Ctsd have been observed. Chen et al. have pointed out that Ctsd serves as an important predictive biomarker in patients who develop HF following acute MI, with its expression level closely correlated with inflammation and collagen metabolism [38]. In general, the high expression expression of Ctsd after MI has a protective effect on the myocardium.

Lgals3, responsible for encoding galectin-3, assumes a significant role in orchestrating inflammatory responses and fibrosis after MI. Notably, SMCs expressing Lgals3 could undergo transition into pro-fibrotic progenitor-like cells [39, 40]. Col3a1 encodes type III collagen. Its increased expression is associated with myocardial fibrosis after MI. Notably, inhibiting TGF-β1 has been shown to attenuate Col3a1 expression, consequently reducing the extent of fibrosis [41, 42]. Consistent with our findings, Lgals3 is highly expressed in macrophages after MI.

The gene Ctsl encoding cathepsin L, assumed regulatory control over the expression of inflammatory cytokines and ECM related genes after MI, as well as the myocardial repair process. The deficiency of Ctsl has been demonstrated to exacerbate cardiac dysfunction in the wake of MI, accentuating its significance in cardiac health [35, 43]. The results showed that macrophages isolated after MI exhibit high expression of Ctsl, suggesting that further investigations may delve into the mechanisms of Ctsl regulation in myocardial repair.

Limitations

We recognized that this study has several limitations. This study analyzed only sequencing datasets and simple in vitro experiments, so sensitivity may be limited. Moreover, to learn more about the metabolic changes induced by MI, we need to explore more time points after MI, such as days 1, 3, 5, 7 and 14. This opens up new opportunities for future research.

Conclusion

To sum up, our comprehensive analysis, integrating bulk RNA-seq and scRNA-seq data, unveiled significant MI-induced shifts in both cellular composition and transcriptional profiles within pivotal cardiac cell populations. The implications of these findings were profound, as they potentially highlight novel therapeutic targets and candidate biomarkers for MI, contingent upon further rigorous validation. Furthermore, the pursuit of more refined scRNA-seq approaches over extended post-MI timeframes stands to provide a meticulously detailed map of the intricate molecular pathways underpinning infarction and the subsequent maladaptive remodeling processes, thus advancing our understanding of MI pathogenesis.

Conclusion

In summary, our study revealed that MI alters the transcriptomic landscapes of cardiac cells, with notable changes in fibroblast subclusters and heightened pro-fibrotic gene expression. Concurrently, we observed a decrease in endothelial cells and evidence of ferroptosis, suggesting its crucial role in MI pathogenesis. Future research should delve deeper into the potential of fibrosis genes as therapeutic targets to develop effective treatment strategies for MI.

Abbreviations

MI	Myocardial infarction
scRNA-seq	Single-cell RNA sequencing
PCA	Principal Component Analysis
LVEF	Left ventricular ejection fraction
LVSF	Left ventricular shortening fraction
IL-10	Interleukin-10
LAD	Left anterior descending coronary artery
PFA	Paraformaldehyde
OCT	Optimal cutting temperature compound
DEG	Differential expression gene
HF	Heart failure
PPI	Protein-protein interaction
GSEA	Gene set enrichment analysis

Supplementary Information

The online version contains supplementary material available at https://doi.org/10.1186/s12864-024-10813-1.

Supplementary Material 1

Supplementary Material 2

Supplementary Material 3

Acknowledgements

Not applicable.

Author contributions

WLL contributed to manuscript writing and performed the experiments, RGJ and LH performed the animal experiments, HCX, CX, SCY, ZHS, TT, YF and YTW analyzed the data, BLZ, and JYY performed the vitro experiments, HQZ, JC, and ZX designed the research, analyzed the data. TL revised the manuscript. All authors read and approved the final manuscript.

Funding

This work was supported by General Project of Key R&D Program of Ganzhou City, Jiangxi Province (202101124510); Natural Science Foundation

of Jiangxi Province (20212BAB216072); Science and Technology Program Project of Jiangxi Provincial Administration of Traditional Chinese Medicine (SZYY2020A0305).

Data availability
The data that support the findings of this study are available. These data were derived from the following resources available in the public domain: [GEO: GSE136088, GSE153485, GSE60993, GSE61144, GSE186079 and GSE123342].

Declarations

Ethical approval
We confirmed that we have followed the ARRIVE guideline. The ethical clearance for our research was secured from the Ethical Committee of Gannan Medical University, under the reference number: 2023555.

Consent for publication
N/A.

Competing interests
The authors declare no competing interests.

Received: 10 April 2024 / Accepted: 19 September 2024
Published online: 03 October 2024

References

1. Li T, Providencia R, Mu N, Yin Y, Chen M, Wang Y, Liu M, Yu L, Gu C, Ma H. Association of metformin monotherapy or combined therapy with cardiovascular risks in patients with type 2 diabetes mellitus. Cardiovasc Diabetol. 2021;20(1):30.
2. Li T, Mu N, Yin Y, Yu L, Ma H. Targeting AMP-Activated protein kinase in aging-related Cardiovascular diseases. Aging Dis. 2020;11(4):967–77.
3. Jiang S, Yang Y, Li T, Ma Z, Hu W, Deng C, Fan C, Lv J, Sun Y, Yi W. An overview of the mechanisms and novel roles of Nrf2 in cardiovascular diseases. Expert Opin Ther Targets. 2016;20(12):1413–24.
4. Li T, Providencia R, Jiang W, Liu M, Yu L, Gu C, Chang ACY, Ma H. Association of Metformin with the Mortality and Incidence of Cardiovascular events in patients with pre-existing Cardiovascular diseases. Drugs. 2022;82(3):311–22.
5. Li T, Jiang S, Lu C, Hu W, Ji T, Han M, Yang Y, Jin Z. Snapshots: endoplasmic reticulum stress in lipid metabolism and Cardiovascular Disease. Curr Issues Mol Biol. 2018;28:14–28.
6. Li T, Yin Y, Mu N, Wang Y, Liu M, Chen M, Jiang W, Yu L, Li Y, Ma H. Metformin-enhanced Cardiac AMP-Activated protein Kinase/Atrogin-1 pathways inhibit charged multivesicular body protein 2B Accumulation in Ischemia-Reperfusion Injury. Front Cell Dev Biol. 2020;8:621509.
7. Tian X, Huang Y, Zhang X, Fang R, Feng Y, Zhang W, Li L, Li T. Salidroside attenuates myocardial ischemia/reperfusion injury via AMPK-induced suppression of endoplasmic reticulum stress and mitochondrial fission. Toxicol Appl Pharmacol. 2022;448:116093.
8. Yang Y, Hu W, Di S, Ma Z, Fan C, Wang D, Jiang S, Li Y, Zhou Q, Li T, et al. Tackling myocardial ischemic injury: the signal transducer and activator of transcription 3 (STAT3) at a good site. Expert Opin Ther Targets. 2017;21(2):215–28.
9. Gao X, Tian X, Huang Y, Fang R, Wang G, Li D, Zhang J, Li T, Yuan R. Role of circular RNA in myocardial ischemia and ageing-related diseases. Cytokine Growth Factor Rev. 2022;65:1–11.
10. Boytsov SA, Shakhnovich RM, Erlikh AD, Tereschenko SN, Kukava NG, Rytova YK, Pevsner DV, Reitblat OM, Konstantinov SL, Kletkina AS, et al. Registry of Acute myocardial infarction. REGION-MI - Russian Registry of Acute myocardial infarction. Kardiologiia. 2021;61(6):41–51.
11. Mohammed AQ, Abdu FA, Liu L, Yin G, Xu B, Xu S, Feng C, Lv X, Fan R, Che W et al. Does sex influence outcomes in myocardial infarction with nonobstructive coronary arteries? Angiology. 2022;73(3):275–80.
12. Ong P, Sechtem U. Diagnostic work-up of patients with myocardial infarction with unobstructed coronary arteries (MINOCA) - practical considerations. Int J Cardiol. 2021;339:14–6.
13. Palacios Ordonez C, Garan AR. The landscape of cardiogenic shock: epidemiology and current definitions. Curr Opin Cardiol. 2022;37(3):236–40.
14. Elbadawi A, Elgendy IY, Omer M, Abdelazeem M, Nambi V, Krittanawong C, Hira RS, Tamis-Holland J, Ballantyne C, Jneid H. Outcomes of Acute myocardial infarction in patients with familial hypercholesteremia. Am J Med. 2021;134(8):992–e10011004.
15. De Luca L, Paolucci L, Nusca A, Putini RL, Mangiacapra F, Natale E, Ussia GP, Colivicchi F, Grigioni F, Musumeci F, et al. Current management and prognosis of patients with recurrent myocardial infarction. Rev Cardiovasc Med. 2021;22(3):731–40.
16. Rasanen M, Sultan I, Paech J, Hemanthakumar KA, Yu W, He L, Tang J, Sun Y, Hlushchuk R, Huan X, et al. VEGF-B promotes endocardium-derived coronary Vessel Development and Cardiac Regeneration. Circulation. 2021;143(1):65–77.
17. Ruiz-Villalba A, Romero JP, Hernandez SC, Vilas-Zornoza A, Fortelny N, Castro-Labrador L, San Martin-Uriz P, Lorenzo-Vivas E, Garcia-Olloqui P, Palacio M, et al. Single-cell RNA sequencing analysis reveals a crucial role for CTHRC1 (Collagen Triple Helix Repeat Containing 1) cardiac fibroblasts after myocardial infarction. Circulation. 2020;142(19):1831–47.
18. Wu X, Fan J, Zhang X, Li T, Song J. Global trends of single cell sequence associated in cancer from 2011 to 2024: a bibliometric analysis. Heliyon. 2024;10(12):e32847.
19. Liu T, Bai M, Liu M, Li T, Liao Y, Zhao C, Yao M, Wang J, Wen A, Ding Y. Novel synergistic mechanism of 11-keto-beta-boswellic acid and Z-Guggulsterone on ischemic stroke revealed by single-cell transcriptomics. Pharmacol Res. 2023;193:106803.
20. Abouleisa RRE, Salama ABM, Ou Q, Tang XL, Solanki M, Guo Y, Nong Y, McNally L, Lorkiewicz PK, Kassem KM, et al. Transient cell cycle induction in Cardiomyocytes to treat Subacute Ischemic Heart failure. Circulation. 2022;145(17):1339–55.
21. Jung SH, Hwang BH, Shin S, Park EH, Park SH, Kim CW, Kim E, Choo E, Choi IJ, Swirski FK, et al. Spatiotemporal dynamics of macrophage heterogeneity and a potential function of Trem2(hi) macrophages in infarcted hearts. Nat Commun. 2022;13(1):4580.
22. Zhang L, Gu S, Wang L, Zhao L, Li T, Zhao X, Zhang L. M2 macrophages promote PD-L1 expression in triple-negative breast cancer via secreting CXCL1. Pathol Res Pract. 2024;260:155458.
23. Tang Z, Wei X, Li T, Wu H, Xiao X, Hao Y, Li S, Hou W, Shi L, Li X, et al. Three-dimensionally printed Ti2448 with low stiffness enhanced angiogenesis and Osteogenesis by regulating macrophage polarization via Piezo1/YAP Signaling Axis. Front Cell Dev Biol. 2021;9:750948.
24. Zhang J, Yang Y, Yang Z, Li T, Chen F. Snapshot: Targeting macrophages as a candidate for tissue regeneration. Curr Issues Mol Biol. 2018;29:37–48.
25. Wu X, Guan S, Lu Y, Xue J, Yu X, Zhang QI, Wang X, Li T. Macrophage-derived SHP-2 inhibits the metastasis of colorectal cancer via Tie2-PI3K signals. Oncol Res. 2023;31(2):125–39.
26. Arai R, Fukamachi D, Ebuchi Y, Migita S, Morikawa T, Monden M, Tamaki T, Kojima K, Akutsu N, Murata N, et al. Mechanical complications of myocardial infarction. Int Heart J. 2021;62(3):499–509.
27. Revelo XS, Parthiban P, Chen C, Barrow F, Fredrickson G, Wang H, Yucel D, Herman A, van Berlo JH. Cardiac Resident macrophages prevent fibrosis and stimulate angiogenesis. Circ Res. 2021;129(12):1086–101.
28. Arif M, Klevstig M, Benfeitas R, Doran S, Turkez H, Uhlen M, Clausen M, Wikstrom J, Zhang C et al. Integrative transcriptomic analysis of tissue-specific metabolic crosstalk after myocardial infarction. Elife 2021;10.
29. Hu J, Liu X, Tang Y. HMGB1/Foxp1 regulates hypoxia-induced inflammatory response in macrophages. Cell Biol Int. 2022;46(2):265–77.
30. Shirakawa K, Endo J, Kataoka M, Katsumata Y, Anzai A, Moriyama H, Kitakata H, Hiraide T, Ko S, Goto S, et al. MerTK expression and ERK Activation are essential for the functional maturation of osteopontin-producing reparative macrophages after myocardial infarction. J Am Heart Assoc. 2020;9(18):e017071.
31. Shirakawa K, Endo J, Kataoka M, Katsumata Y, Yoshida N, Yamamoto T, Isobe S, Moriyama H, Goto S, Kitakata H, et al. IL (Interleukin)-10-STAT3-Galectin-3 Axis is essential for osteopontin-producing reparative macrophage polarization after myocardial infarction. Circulation. 2018;138(18):2021–35.
32. Duscher D, Maan ZN, Whittam AJ, Sorkin M, Hu MS, Walmsley GG, Baker H, Fischer LH, Januszyk M, Wong VW, et al. Fibroblast-specific deletion of Hypoxia Inducible Factor-1 critically impairs murine cutaneous neovascularization and Wound Healing. Plast Reconstr Surg. 2015;136(5):1004–13.
33. Hoeft K, Schaefer GJL, Kim H, Schumacher D, Bleckwehl T, Long Q, Klinkhammer BM, Peisker F, Koch L, Nagai J, et al. Platelet-instructed SPP1(+) macrophages drive myofibroblast activation in fibrosis in a CXCL4-dependent manner. Cell Rep. 2023;42(2):112131.

34. Qiao S, Zhao WJ, Li HQ, Ao GZ, An JZ, Wang C, Zhang HL. Necrostatin-1 Analog DIMO exerts cardioprotective effect against Ischemia Reperfusion Injury by suppressing necroptosis via Autophagic Pathway in rats. Pharmacology. 2021;106(3–4):189–201.
35. Kanamori H, Takemura G, Goto K, Maruyama R, Tsujimoto A, Ogino A, Takeyama T, Kawaguchi T, Watanabe T, Fujiwara T, et al. The role of autophagy emerging in postinfarction cardiac remodelling. Cardiovasc Res. 2011;91(2):330–9.
36. Sun M, Chen M, Liu Y, Fukuoka M, Zhou K, Li G, Dawood F, Gramolini A, Liu PP. Cathepsin-L contributes to cardiac repair and remodelling post-infarction. Cardiovasc Res. 2011;89(2):374–83.
37. Wu P, Yuan X, Li F, Zhang J, Zhu W, Wei M, Li J, Wang X. Myocardial upregulation of cathepsin D by Ischemic Heart Disease promotes autophagic flux and protects against Cardiac Remodeling and Heart failure. Circ Heart Fail 2017;10(7).
38. Chen Q, Yin Q, Song J, Liu C, Chen H, Li S. Identification of monocyte-associated genes as predictive biomarkers of heart failure after acute myocardial infarction. BMC Med Genomics. 2021;14(1):44.
39. Owsiany KM, Deaton RA, Soohoo KG, Tram Nguyen A, Owens GK. Dichotomous roles of smooth muscle cell-derived MCP1 (monocyte chemoattractant protein 1) in development of atherosclerosis. Arterioscler Thromb Vasc Biol. 2022;42(8):942–56.
40. Yokota T, McCourt J, Ma F, Ren S, Li S, Kim TH, Kurmangaliyev YZ, Nasiri R, Ahadian S, Nguyen T, et al. Type V Collagen in scar tissue regulates the size of scar after Heart Injury. Cell. 2020;182(3):545–e562523.
41. Hodges MM, Zgheib C, Xu J, Hu J, Dewberry LC, Hilton SA, Allukian MW, Gorman JH 3rd, Gorman RC, Liechty KW. Differential expression of transforming growth Factor-beta1 is Associated with fetal regeneration after myocardial infarction. Ann Thorac Surg. 2019;108(1):59–66.
42. Loi H, Kramar S, Laborde C, Marsal D, Pizzinat N, Cussac D, Roncalli J, Boal F, Tronchere H, Oleshchuk O et al. Metformin attenuates postinfarction myocardial fibrosis and inflammation in mice. Int J Mol Sci. 2021;22(17).
43. Meijers WC, van der Velde AR, Pascual-Figal DA, de Boer RA. Galectin-3 and post-myocardial infarction cardiac remodeling. Eur J Pharmacol. 2015;763(Pt A):115–21.

Publisher's note